



ORIGINAL RESEARCH

Ovarian Tumor Domain-Containing 7B Attenuates Pathological Cardiac Hypertrophy by Inhibiting Ubiquitination and Degradation of Krüppel-Like Factor 4

Bin-Bin Du, MD*¹; Jie-Lei Zhang, MD, PhD*¹; Ling-Yao Kong, MD, PhD*¹; Hui-Ting Shi, MD; Dian-Hong Zhang, MD, PhD; Xing Wang, MD; Chun-Lei Yang , MD; Peng-Cheng Li, MD, PhD; Rui Yao, MD, PhD; Cui Liang, MD; Lei-Ming Wu, MD, PhD; Zhen Huang , MD

BACKGROUND: Cardiac hypertrophy (CH) is a well-established risk factor for many cardiovascular diseases and a primary cause of mortality and morbidity among older adults. Currently, no pharmacological interventions have been specifically tailored to treat CH. OTUD7B (ovarian tumor domain-containing 7B) is a member of the ovarian tumor-related protease (OTU) family that regulates many important cell signaling pathways. However, the role of OTUD7B in the development of CH is unclear. Therefore, we investigated the role of OTUD7B in CH.

METHODS AND RESULTS: OTUD7B knockout mice were used to assay the role of OTUD7B in CH after transverse aortic coarctation surgery. We further assayed the specific functions of OTUD7B in isolated neonatal rat cardiomyocytes. We found that OTUD7B expression decreased in hypertrophic mice hearts and phenylephrine-stimulated neonatal rat cardiomyocytes. Furthermore, OTUD7B deficiency exacerbated transverse aortic coarctation surgery-induced myocardial hypertrophy, abnormal cardiac function, and fibrosis. In cardiac myocytes, OTUD7B knockdown promoted phenylephrine stimulation-induced myocardial hypertrophy, whereas OTUD7B overexpression had the opposite effect. An immunoprecipitation–mass spectrometry analysis showed that OTUD7B directly binds to KLF4 (Krüppel-like factor 4). Additional molecular experiments showed that OTUD7B impedes KLF4 degradation by inhibiting lysine residue at 48 site-linked ubiquitination and suppressing myocardial hypertrophy by activating the serine/threonine kinase pathway.

CONCLUSIONS: These results demonstrate that the OTUD7B-KLF4 axis is a novel molecular target for CH treatment.

Key Words: AKT signaling pathway ■ cardiac hypertrophy ■ KLF4 ■ ovarian tumor domain-containing 7B

Cardiac hypertrophy (CH) is a compensatory and adaptive mechanism that preserves cardiac output during detrimental stimuli and an independent risk factor for cardiovascular mortality globally.¹ During the initial stages, CH is associated with normal or enhanced cardiac function and considered adaptive or physiological. During later stages, if the stimulus

is not removed, then it is associated with contractile dysfunction and termed pathological CH.² Notably, oxidative stress,³ inflammatory processes,⁴ mitochondrial dysfunction,⁵ and apoptosis⁶ in cardiomyocytes have been suggested to play critical roles in contractile function depression during pathological hypertrophy development.^{7,8} Cellularly, cardiomyocyte hypertrophy

Correspondence to: Lei-Ming Wu, MD, PhD, and Zhen Huang, MD, Cardiovascular Hospital, First Affiliated Hospital of Zhengzhou University, Zhengzhou University, No.1 Jianshe East Road, Zhengzhou, Henan 450052, China. Email: wyzsry1983@163.com, huangzhen0037@163.com

*B.-B. Du, J.-L. Zhang, and L.-Y. Kong contributed equally.

This article was sent to Rebecca D. Levit, MD, Associate Editor, for review by expert referees, editorial decision, and final disposition.

Supplemental Material is available at <https://www.ahajournals.org/doi/suppl/10.1161/JAHA.123.029745>

For Sources of Funding and Disclosures, see page 15.

© 2023 The Authors. Published on behalf of the American Heart Association, Inc., by Wiley. This is an open access article under the terms of the [Creative Commons Attribution-NonCommercial-NoDerivs](https://creativecommons.org/licenses/by-nc-nd/4.0/) License, which permits use and distribution in any medium, provided the original work is properly cited, the use is non-commercial and no modifications or adaptations are made.

JAHA is available at: www.ahajournals.org/journal/jaha

RESEARCH PERSPECTIVE

What Is New?

- OTUD7B (ovarian tumor domain-containing 7B) protects against pressure overload-induced cardiac hypertrophy.
- OTUD7B directly binds to KLF4 (Krüppel-like factor 4) and impedes its degradation by inhibiting lysine residue at 48 site-linked ubiquitination and suppressing cardiac hypertrophy by activating the serine/threonine kinase pathway.

What Question Should Be Addressed Next?

- Further studies are needed to refine the study of OTUD7B overexpression on cardiac hypertrophy in vivo and establish a molecular role for OTUD7B and KLF4 in the regulation of cardiac remodeling and the progression of cardiac hypertrophy.

Nonstandard Abbreviations and Acronyms

AKT	serine/threonine kinase
CH	cardiac hypertrophy
Ctgf	connective tissue growth factor
KLF4	Krüppel-like factor 4
KO	knockout
NRCM	neonatal rat cardiomyocyte
OTUD7B	ovarian tumor domain-containing 7B
Postn	periosteum protein
TAC	transverse aortic coarctation
TGF-β	transforming growth factor- β

is characterized by enlarged cell size, enhanced protein synthesis, and increased sarcomere organization. Exploring effective and promising therapeutic targets may lead to the prevention of adverse outcomes. Moreover, a better understanding of the mechanisms underlying CH may lead to novel therapeutic approaches to reverse adverse pathologies.

Several mechanisms have been highlighted as potential contributors to the etiopathogenesis of CH, primarily based on the typical knowledge of molecular regulation.⁹ Conversely, signaling pathways related to protein kinases (such as protein kinase A),¹⁰ as well as the activation of MAPK (mitogen-activated protein kinase) and JNK (c-Jun N-terminal kinase), also contribute to pathological hypertrophic maladaptive gene expression. Moreover, mTOR (mammalian target of rapamycin), NF- κ B (nuclear factor κ B), and calcineurin

signaling pathways play vital roles in CH.^{11–13} Notably, mibefradil alleviates high-glucose-induced CH by inhibiting PI3K (phosphatidylinositol 3-kinase)/PKB (protein kinase B, also known as AKT [serine/threonine kinase])/mTOR-mediated autophagy.¹⁴ Isorhamnetin protects against CH by blocking the PI3K-AKT pathway.¹⁵ Although the aforementioned signaling pathways have been extensively characterized in pressure overload, it is crucial to improving understanding of the mechanisms responsible for CH. Therefore, new molecular pathways involved in AKT signaling should be considered as potential therapeutic targets for CH.

OTUD7B (ovarian tumor domain-containing 7B) is a member of the ovarian tumor protease (OTU) family, which plays a pivotal role in the regulation of crosstalk between inflammation, autophagy, oxidative stress, apoptosis, and innate immune signaling; however, its regulatory mechanisms are poorly understood.^{16,17} Molecularly, OTUD7B inhibits LCL161 inhibitor of apoptosis protein antagonist-induced invasion and migration by binding to and deubiquitinating TRAF3 (tumor necrosis factor receptor-associated factor 3), thereby inhibiting NIK (NF- κ B-inducing kinase) and preventing noncanonical NF- κ B activation in lung cancer.¹⁸ TRAF2 and OTUD7B regulate a ubiquitin-dependent switch that controls mTORC2 (mammalian target of rapamycin complex 2) signaling during lung tumorigenesis.¹⁹ Furthermore, OTUD7B stabilizes estrogen receptor- α and promotes breast cancer cell proliferation.²⁰ MicroRNA-486-5p promotes acute lung injury by inducing inflammation and apoptosis by targeting OTUD7B.²¹ Moreover, OTUD7B promotes tumor progression via the AKT/VEGF (vascular endothelial growth factor) pathway in lung squamous carcinoma and adenocarcinoma.²² Recently, studies have shown that OTUD7B is a cell-cycle-regulated deubiquitinase that antagonizes the degradation of APC/C (anaphase-promoting complex or cyclosome) substrates. Screening of a large collection of recombinant deubiquitinating enzymes (DUBs) using a panel of deubiquitin probes revealed that a subfamily containing the OTU domain exhibited ubiquitin linkage specificity. Conflicting reports of 1 of these enzymes, OTUD7B, indicated its ability to disassemble lysine residue at site 11-linked chains²³ as well as lysine residue at 48 site (K48)-linked and lysine residue at site 63-linked ubiquitin chains.²⁴ However, the exact molecular factors and mechanisms underlying OTUD7B ubiquitination are largely unexplored, and the precise function of OTUD7B in CH remains unclear. Therefore, we investigated the role of OTUD7B in CH.

In the present study, we found that OTUD7B expression was markedly decreased during CH development. Through gain-of-function and loss-of-function studies in vitro and in vivo, we demonstrated the protective role of OTUD7B in CH. Notably, OTUD7B suppressed

CH progression by activating AKT signaling cascades and regulating KLF4 (Krüppel-like factor 4) degradation. Collectively, our findings suggest that OTUD7B is a potential therapeutic target for CH.

METHODS

The authors declare that all supporting data are available within the article and its online supplementary files.

Construction of Animal Models

All animal experiments were approved by the Ethics Committee of the First Affiliated Hospital of Zhengzhou University. All procedures were performed in accordance with the National Institutes of Health Guidelines for the Care and Use of Laboratory Animals.

To obtain OTUD7B knockout (KO) mice, the guide sequence of the target DNA region was predicted using the clustered regularly interspaced short palindromic repeats (CRISPR) online design tool (<http://chopchop.cbu.uib.no/>). The guide RNA target site was CAGTTGCGTCAAGTCCATGCTGG, and pUC57-sgRNA (51 132; Addgene) was used as the backbone vector to construct the OTUD7B-sgRNA expression vector. The *in vitro* transcriptional purification products of both the Cas9 (CRISPR-associated protein 9) expression vector pST1374-Cas9 (44 758; Addgene) and sgRNA expression vector were mixed. Then, the mixture was injected into single-cell fertilized eggs of C57BL/6J mice using a FemtoJet 5247 microinjection system. The founder generation mice were obtained after ~19 to 21 days of gestation. Teo tissues were removed from mice 2 weeks after birth. Genomic DNA was extracted, and the following primers were used to identify the genotypes of mice: 5'-ATGGTCTTCTGTGTCCTCCC-3' (OTUD7B-check F1) and 5'-TCTAAAGGAGCACACAGGCG-3' (OTUD7B-check R1). Subsequently, the selected founder lines were multiplied and constructed until OTUD7B^{-/-} mice were obtained for subsequent experiments.

Animal Surgery

Male KO and wild-type (WT) mice (weight, 25.5–27 g; age, 9–11 weeks) were selected and randomly divided into the transverse aortic coarctation (TAC) and sham surgery groups (n=6 per group). Briefly, male mice were anesthetized with sodium pentobarbital via intraperitoneal injection, and the left side of the chest was opened to expose the aortic arch through the second intercostal space after the toe pinch reflex disappeared. Subsequently, the thoracic aorta was ligated with a 7–0 silk suture using a 27-gauge needle, which was rapidly removed before the closure of the thoracic cavity. A Doppler analysis was performed to evaluate

the aortic constriction level. Notably, the animals in the sham surgery group underwent every procedure except ligation of the aorta. All surgical procedures were performed in a blinded manner.

Echocardiographic Assessment

Echocardiography was performed using a small animal ultrasound imaging system (VEVO2100; Fujifilm Visualsonics, Toronto, Ontario, Canada) with a 30-MHz (MS400) probe. The mice were continuously anesthetized with isoflurane (1.5%–2%). The left ventricular (LV) cavity volume and LV wall thickness were obtained from at least 3 consecutive cardiac cycles. End-systole and end-diastole were defined as phases in which the smallest and largest LV areas were acquired, respectively. M-mode tracings were derived from the LV end-diastolic dimension, LV end-systolic dimension, and ejection fraction percent, scanning with 50 mm/s at the mid-papillary muscle level. Fraction shortening percent was calculated using the following formula: fraction shortening percent=[LV end-diastolic dimension–LV end-systolic dimension]/LV end-diastolic dimension×100%.

Animal Materials

Four weeks after TAC surgery, to obtain their weight, the mice were euthanized and weighed. After the heart was removed, it was quickly placed in 10% KCl solution to stop the heart in diastole. The heart was weighed and fixed in liquid nitrogen or 10% formalin, and the tibial length was measured simultaneously.

Histomorphological Analysis

After the hearts were fixed for 48 hours, we performed serial sections of cross-sectioned heart wax blocks (section thickness, 5 μm). After staining with hematoxylin (G1004; Servicebio), eosin (BA-4024; Baso), and picric acid Sirius scarlet (picrosirius red; 26357–02; Hedebiototechnology), the cross-sectional area of the cardiomyocytes and collagen fiber content were measured individually using Image-Pro Plus 6.0 software.

Western Blotting Analysis

The removed LV tissue or cell samples were lysed by adding RIPA lysate (720 μL of RIPA buffer, 20 μL of phenylmethylsulfonyl fluoride, 100 μL of complete protease inhibitor cocktail, 100 μL of Phos-stop, 50 μL of NaF, and 10 μL of Na₃VO₄; final volume of 1 mL). After lysis and centrifugation, the supernatant was collected as the total protein and quantified using a bicinchoninic acid protein kit (Pierce). The same protein mass was separated using 10% SDS-PAGE and transferred to 0.45 μm polyvinylidene fluoride membranes (IPVH00010; Millipore); subsequently, it was sealed with

5% skim milk powder for 1 hour at 25 °C. The polyvinylidene fluoride membranes were washed 3 times with TBST 20 for 5 minutes each. Primary antibodies were added and incubated at 4 °C overnight. Secondary antibodies against the corresponding species (Jackson ImmunoResearch) were added the following day after washing with tris-buffered saline with Tween 20. We used an electrochemiluminescence luminescent substrate (1705062; Bio-Rad) for color development and a Burroughs gel imaging system (ChemiDoc XRS+) for signal collection. Image Lab (version 5.1) software was used to analyze the results (Table S1).

Quantitative Reverse Transcription-Polymerase Chain Reaction

Total RNA was extracted by adding the removed LV tissue or cell samples to the TRIZOL reagent (15596-026; Invitrogen). RNA was reverse-transcribed to cDNA using the Transcriptor First Strand cDNA Synthesis Kit (04896866001; Roche). The SYBR Green Polymerase Chain Reaction Master Mix (04887352001; Roche) was added to a specific system to detect the expression of the gene to be tested using reverse transcription-polymerase chain reaction (Roche). Additionally, *GAPDH* was used as an internal reference gene. The primers used for sequencing are listed in Table S2.

Adenovirus Construction

The overexpression OTUD7B adenovirus for the rats was purchased from Hanheng Biotechnology (Shanghai, China). OTUD7B adenovirus knockdown was completed by constructing a replication-deficient adenovirus vector carrying a short hairpin RNA targeting OTUD7B, whereas an adenovirus vector carrying a short hairpin RNA (AdshRNA) was used as a control. Overexpressing KLF4 adenovirus was also constructed, and a green fluorescent protein (GFP)-expressing adenovirus was used as a control. Adenoviruses were used to infect cardiomyocytes at a multiplicity of infection of 50 particles per cell for 24 hours, followed by assay identification (Table S3).

Plasmid Constructs

Full-length or truncated OTUD7B, KLF4, Myc-K48O (myelocytomatosis-lysine [K] 48 only), and Myc-K48R (lysine [K] 48 mutated to arginine [R]) were amplified from human cDNA and ligated into different vectors to obtain overexpression plasmids using the infusion method (Table S3).

Cardiomyocyte Isolation and Culture

The hearts of 1- to 2-day-old Sprague-Dawley rats were cut into 1- to 2-mm³ size after removing nonheart

tissue. Subsequently, the tissue was digested with 0.125% trypsin to obtain neonatal rat cardiomyocytes (NRCMs), which were incubated with DMEM/F12 (C11330; Gibco), 10% fetal bovine serum (10099141C; Gibco), 1% penicillin/streptomycin, and 5-bromodeoxyuridine (0.1 mmol/L to inhibit fibroblast proliferation; B5002-250MG; Sigma) for 24 hours. NRCMs were starved in a serum-free medium for 12 hours after infection with adenovirus for 6 hours. Subsequently, NRCMs were stimulated with 50 μmol/L phenylephrine for 24 hours, and an equal amount of PBS was added to the control. The entire cell culture was conducted at 37 °C and 5% CO₂.

Immunofluorescence Staining

NRCMs were cultured for 24 hours, fixed in 4% formaldehyde (G1101-500 mL; Servicebio) for 30 minutes, permeabilized with 0.2% Triton X-100, and blocked with 8% goat serum at 37 °C. The cells were incubated with α-actin antibody (1:100 dilution; 05-384; Merck Millipore), followed by staining with a secondary antibody (1:200 dilution; donkey anti-mouse immunoglobulin G heavy and light chains [H+L] secondary antibody; A21202; Invitrogen). Then, they were incubated on slides containing 4'-diamidino-2-phenylindole. The surface area of the cardiomyocytes was measured using Image-Pro Plus 6.0.

Transcriptome Analysis

For RNA sequencing, total RNA was first extracted from the samples, a cDNA library was constructed, and a single-end library was sequenced using an MGISEQ-2000 RS with a read length of 50 bp. HISAT240 software (version 2.1.0) was used to compare the sequence fragments to the mouse reference genome (mm10/GRCm38). The files obtained using these procedures were converted to the binary alignment map (BAM) format using SAM tools, which can store the alignment information. Fragments per kilobase of the exon model per million mapped fragment values were calculated using the StringTie's default parameters for each identified gene. DESeq2 identified differentially expressed genes based on the following criteria: (1) fold-change >2 and (2) corresponding corrected *P*<0.05.

Hierarchical Clustering Analysis

All gene expression matrix data were analyzed using a hierarchical cluster analysis. This analysis builds hierarchical nested clustering trees by calculating the similarity between different samples using the unweighted pair group method with the arithmetic mean algorithm (UPGMA) and then visualizing them using the hclust function of the R package.

Gene Set Enrichment Analysis

Genes were sorted using gene set enrichment analysis according to their expression levels. Gene sets were examined to determine whether they were concentrated at the top or bottom of the sorting list to investigate overall expression changes based on the Gene Ontology database. A Java Gene set enrichment analysis was performed to obtain the Signal2Noise metric. Gene sets with $P < 0.05$ and a false discovery rate < 0.25 were considered statistically significant.

Kyoto Encyclopedia of Genes and Genomes Enrichment Analysis

The Kyoto Encyclopedia of Genes and Genomes is a comprehensive database containing genomic, chemical, and phylogenetic functional information. Kyoto Encyclopedia of Genes and Genomes pathway annotations for all genes in the reference genome were also downloaded from the Kyoto Encyclopedia of Genes and Genomes database, which defines pathways with $P < 0.05$ as significantly enriched pathways.

Coimmunoprecipitation, Mapping, and Ubiquitination

Human embryonic kidney 293T (HEK293T) cells were cotransfected with the indicated plasmids, whereas primary cardiomyocytes (NRCMs) were infected with the corresponding adenovirus (Table S3). Cells were lysed with cold immunoprecipitation buffer (20 mmol/L Tris-HCl [pH 7.4], 150 mmol/L NaCl, 1 mmol/L EDTA, and 1% NP-40) after the plasmids were transfected for 24 hours. Samples were centrifuged at high speed; the supernatants were then incubated with protein A/G agarose beads and indicated antibody at 4 °C overnight. Subsequently, the beads were washed with 300 mmol/L and 150 mmol/L NaCl buffer 3 times, individually, and boiled with 2× SDS loading buffer at 95 °C for 5 to 10 minutes before Western blotting (WB) analysis.

Glutathione S-Transferase Pull-Down

HEK293T cells were transfected with Flag-tagged or GST (glutathione S-transferase)-influenza hemagglutinin epitope (HA)-tagged plasmids for 24 hours. Subsequently, the cells were collected and lysed with a lysis buffer (50 mmol/L Na_2HPO_4 [pH 8.0], 300 mmol/L NaCl, 1% TritonX-100, protease inhibitor cocktail). After cryogenic centrifugation, GST-HA-tagged proteins were incubated overnight at 4 °C with Flag-tagged proteins purified from GST beads. Subsequently, the beads were washed with buffer (20 mmol/L, 150 mmol/L NaCl, 0.2% TritonX-100) 3 times and boiled with 2× SDS loading buffer at 95 °C for 10 minutes before WB analysis.

Statistical Analysis

All data are presented as the mean±SD. Analysis was performed with SPSS 25.0. Briefly, when the data conformed to a normal distribution, data from 2 groups were analyzed using a 2-tailed Student *t* test. The significant differences among multiple comparisons involving experiments with 3 or more groups were analyzed using 1-way or 2-way ANOVA with Tukey post hoc analysis. For data analyzed by ANOVA, post hoc Bonferroni correction was performed to adjust for multiple comparisons when the data exhibited homogeneity of variance, and the Tamhane T2 (M) post hoc method was used when the data exhibited heterogeneity of variance. For data with skewed distribution, the Mann-Whitney *U* test was used for the nonparametric statistical analysis between the 2 groups. Multiple comparisons were performed using the Kruskal-Wallis test for pairwise comparisons. $P < 0.05$ was defined as statistically significant.

RESULTS

OTUD7B Expression Is Downregulated in CH

To investigate the expression of OTUD7B in CH, NRCMs were treated with phenylephrine to establish myocardial hypertrophy in vitro. In regard to OTUD7B, although the mRNA expression levels of mRNA exhibited no significant differences between PBS and phenylephrine treatment, WB analysis clearly demonstrated that protein expression continued to decrease significantly in the myocardial hypertrophy models (Figure 1A and 1B). Similar results were obtained after TAC surgery was performed in WT mice (Figure 1C and 1D). Furthermore, immunohistochemical test results showed that the expression of OTUD7B was significantly downregulated in the heart of WT mice treated with TAC (Figure 1E). Collectively, the decreased expression of OTUD7B in CH samples suggests that OTUD7B may be involved in the pathogenesis of CH.

OTUD7B Deficiency Aggravates TAC-Induced Cardiac Remodeling

We constructed OTUD7B gene KO mice (Figure S1) for loss-of-function experiments (Figure 2A) to assess whether OTUD7B is involved in CH adjustment. OTUD7B-deficient mice exhibited significant effects on heart weight, lung weight, heart weight/body weight ratio, lung weight/body weight ratio, and heart weight/tibia length ratio after TAC surgery (Figure 2C, 2D, 2F through 2H), rather than on body weight and tibia length (Figure 2B and 2E). With a consistent heart rate in the 4 groups during echocardiography compared with WT mice, cardiac dysfunction deteriorated in OTUD7B KO mice, which was manifested by a significant increase

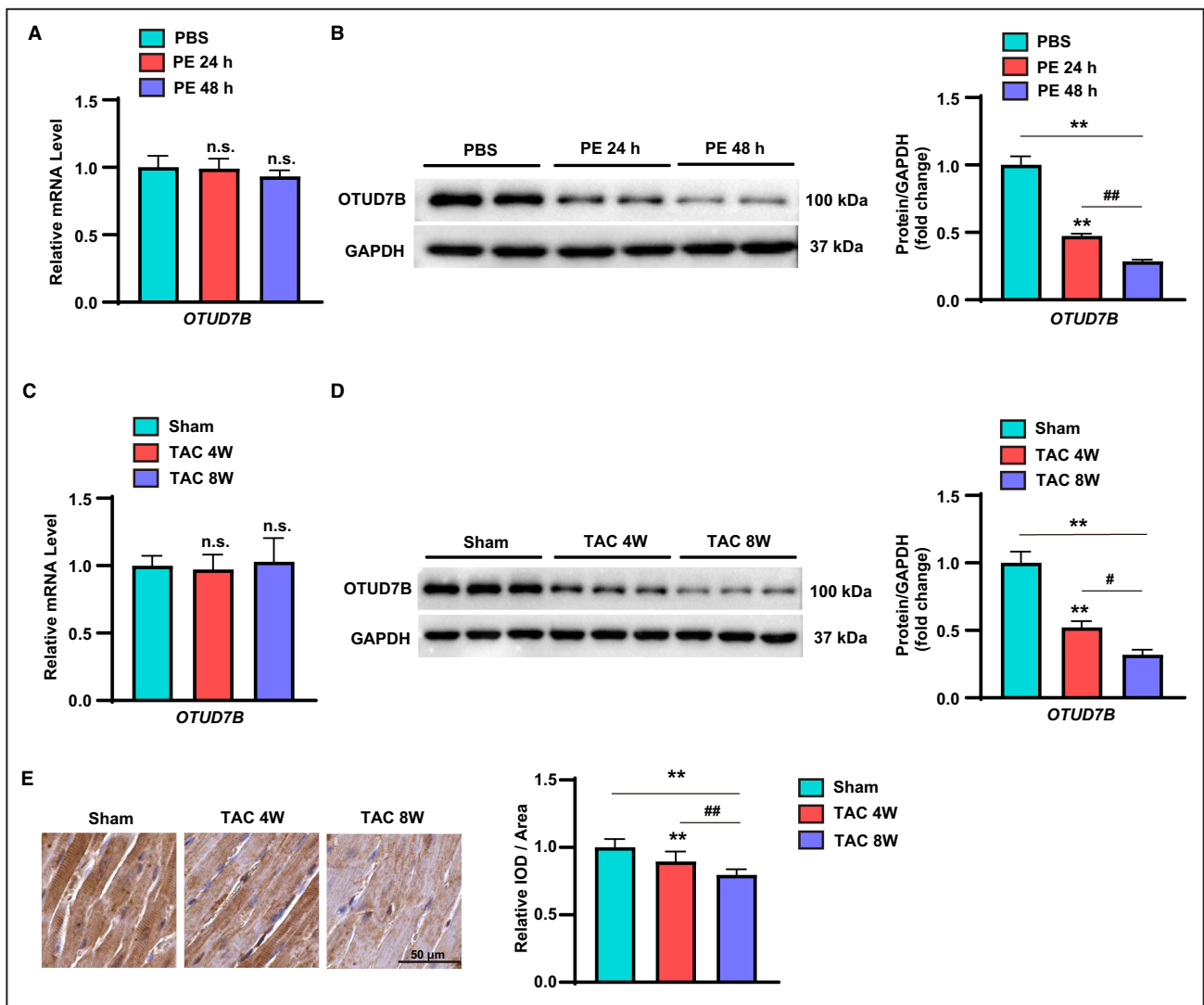


Figure 1. OTUD7B expression is downregulated in cardiac hypertrophy.

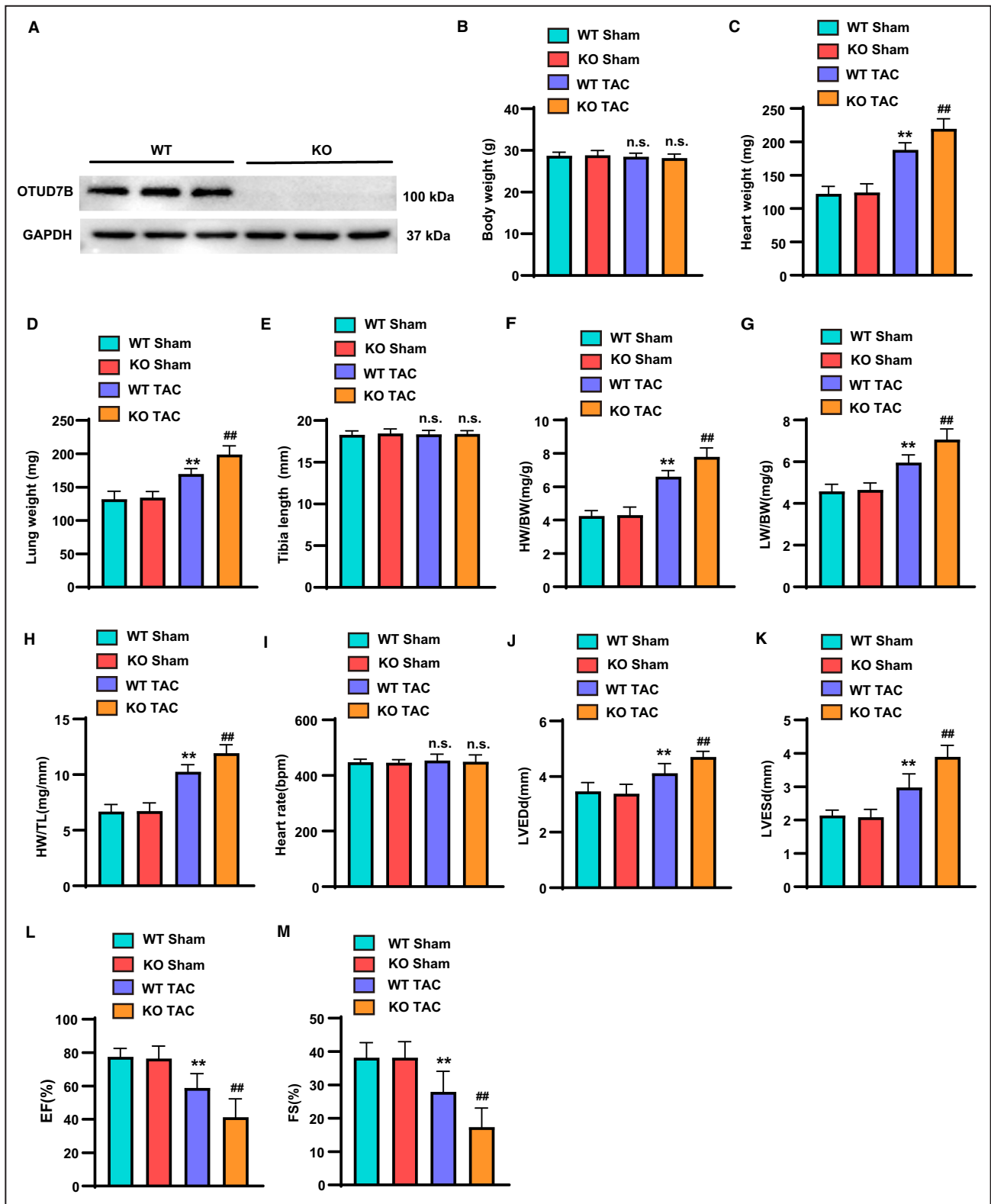
A, RT-PCR analysis of the OTUD7B level in NRCMs treated with PBS or PE for 24 or 48hours. **B**, WB analysis of OTUD7B levels in NRCMs after 24 or 48 hours of PE or PBS treatment. **C**, RT-PCR analysis of the mRNA levels of OTUD7B in mice heart tissues at 4 or 8 weeks after TAC or sham surgery (n=5 mice per group). **D**, WB analysis of OTUD7B levels in mice hearts at 4 or 8 weeks after TAC or sham surgery. **E**, Immunohistochemical staining showed the expression of OTUD7B in mice hearts after TAC or sham surgery (n=3 mice per group). Scale bars: 50µm. **A** through **E**, n.s. or $P>0.05$ vs PBS or sham. $*P<0.05$ or $**P<0.01$ vs PBS or sham. $\#P<0.05$ or $##P<0.01$ vs PE for 24 hours or 4 weeks after TAC. Data are presented as mean±SD. Statistical analysis was conducted using 1-way ANOVA. IOD indicates integrated optical density; NRCMs, neonatal rat cardiomyocytes; n.s., not significant; OTUD7B, ovarian tumor domain-containing 7B; PE, phenylephrine; RT-PCR, reverse transcription-polymerase chain reaction; TAC, transverse aortic coarctation; W, weeks; WB, Western blotting.

in the LV end-diastolic dimension and LV end-systolic dimension, as well as decreased ejection fraction and fraction shortening after TAC surgery (Figure 2I through

2M). These results showed that OTUD7B deficiency significantly exacerbated TAC-induced cardiac dilation and dysfunction.

Figure 2. OTUD7B deficiency aggravates TAC-induced cardiac remodeling.

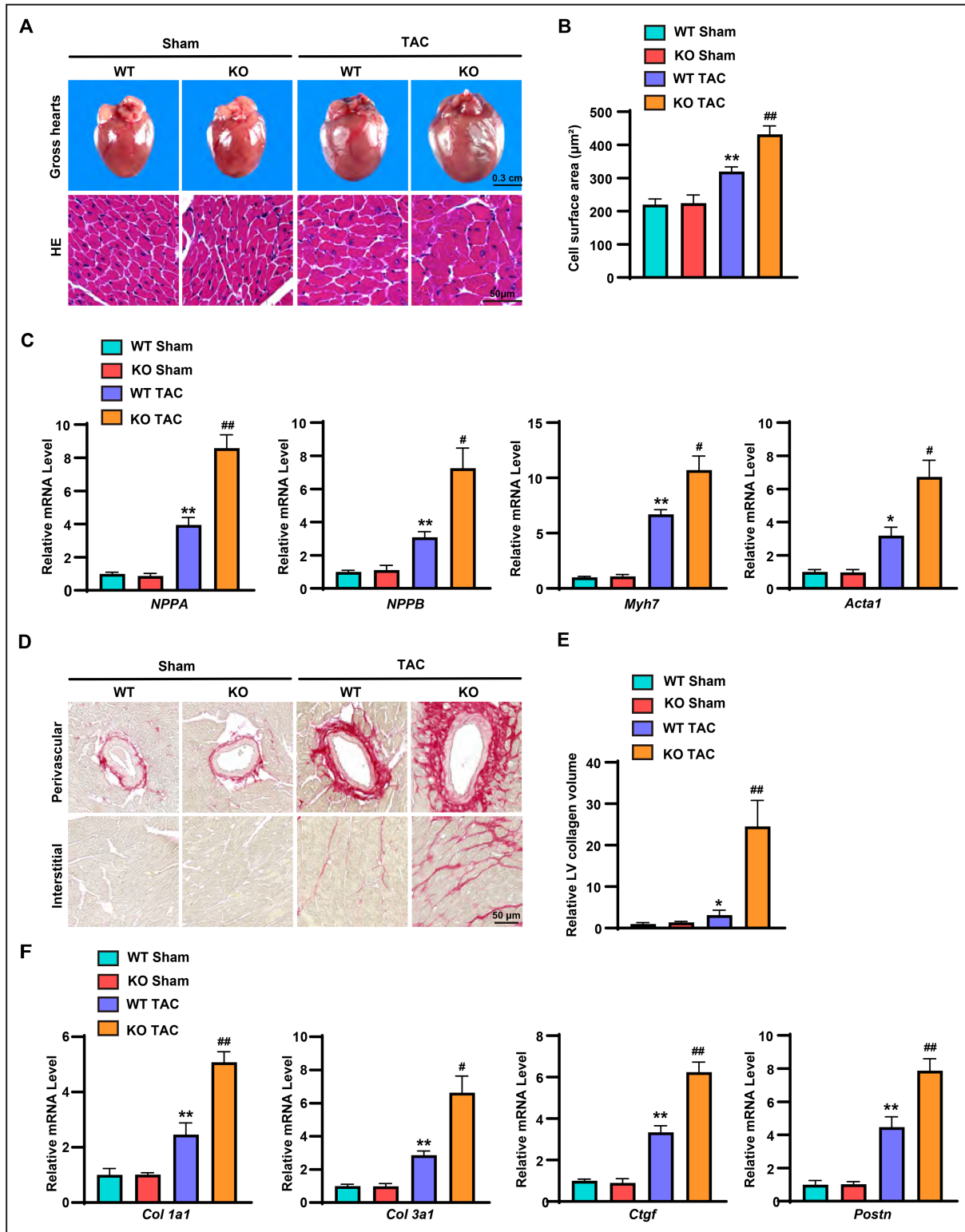
A, WB showed the expression of OTUD7B in the hearts of OTUD7B KO and WT mice. **B** through **H**, Statistical results of the BW, HW, LW, TL, HW/BW ratio, LW/BW ratio, and HW/TL ratio of the indicated groups (n=10 mice per group). **I** through **M**, Control of consistent heart rate in indicated groups during echocardiography measurement, LVEDd, LVESd, EF, and FS showed in the indicated groups (n=10 mice per group). For (**B** through **M**) n.s. or $P>0.05$ vs WT sham or WT TAC. $**P<0.01$ vs WT sham. $##P<0.01$ vs WT TAC. Data are presented as mean±SD. **B** through **D**, and **F** through **M**, Data were statistically analyzed using 1-way ANOVA. **E**, Data were statistically analyzed using a nonparametric test. BW indicates body weight; EF, ejection fraction; FS, fraction shortening; HW, heart weight; KO, knockout; LVEDd, left ventricular end-diastolic dimension; LVESd, left ventricular end-systolic dimension; LW, lung weight; n.s., not significant; OTUD7B, ovarian tumor domain-containing 7B; TAC, transverse aortic coarctation; TL, tibia length; WB, Western blotting; WT, wild-type.



OTUD7B Deficiency Aggravates TAC-Induced CH and Myocardial Fibrosis

Cardiac tissues of the mice were collected 4 weeks after TAC surgery for pathological section staining.

Histological examination results revealed that the gross heart and cross-sectional area of cardiomyocytes in OTUD7B KO mice were higher than those in WT mice 4 weeks after TAC surgery (Figure 3A and 3B). Additionally, compared with WT mice, OTUD7B KO mice exhibited



significantly increased mRNA expression levels of marker genes for CH (*NPPA*, *NPPB*, *Myh7*, and *Acta1*) in the heart tissue after TAC surgery (Figure 3C). These data provide further evidence that the deletion of OTUD7B promoted cardiac remodeling upon pressure

overload. Because perivascular and interstitial fibrosis are crucial features of CH caused by pressure overload, TAC-induced myocardial fibrosis was evaluated using picrosirius red staining to determine the fibrosis degree. After TAC, both perivascular and interstitial

Figure 3. OTUD7B deficiency aggravates TAC-induced cardiac hypertrophy and myocardial fibrosis.

A, Gross hearts and HE staining of WT and OTUD7B KO mice heart tissues at 4 weeks after TAC or sham surgery (n=6 mice per group). Scale bars: 0.3 cm, 50 μ m. **B**, Statistical results of the cell surface area of cardiomyocytes in different groups after HE staining (n=6 mice per group). **C**, RT-PCR analysis of the mRNA levels of *NPPA*, *NPPB*, *Myh7*, and *Acta1* in WT and OTUD7B KO mice at 4 weeks after TAC or sham surgery (n=4 mice per group). **D**, PSR staining of WT and OTUD7B KO mice at 4 weeks after TAC or sham surgery and the degree of perivascular and interstitial fibrosis in mice heart tissues (n=6 mice per group). Scale bars: 50 μ m. **E**, Statistical results of the collagen volume in the left ventricular interstitial tissues in indicated groups (n=6 mice per group). **F**, RT-PCR analysis of the mRNA levels of collagen 1a1, collagen 3a1, *Ctgf*, and *Postn* in WT and OTUD7B KO mice at 4 weeks after TAC or sham surgery (n=4 mice per group). **B** and **C**, **E** and **F**, * P <0.05 or ** P <0.01 vs WT sham. # P <0.05 or ## P <0.01 vs WT TAC. Data are presented as mean \pm SD. Statistical analysis was conducted using 1-way ANOVA. *Ctgf* indicates connective tissue growth factor; HE, hematoxylin-eosin staining; KO, knockout; OTUD7B, ovarian tumor domain-containing 7B; *Postn*, periosteum protein; PSR, picrosirius red; RT-PCR, reverse transcription-polymerase chain reaction; TAC, transverse aortic coarctation; and WT, wild-type.

fibrosis were markedly increased in WT mice; however, these indicators were more pronounced in OTUD7B KO mice (Figure 3D and 3E). Furthermore, the mRNA expression levels of fibrosis markers (collagen 1a1, collagen 3a1, *Ctgf* [connective tissue growth factor], and *Postn* [periosteum protein]) were significantly upregulated in the KO TAC group, revealing that TAC-induced OTUD7B KO mice had significantly more fibrosis than WT mice (Figure 3F). These data provided further evidence that OTUD7B deficiency promotes cardiac remodeling and fibrosis.

OTUD7B Deficiency Aggravates Cardiomyocyte Hypertrophy In Vitro

Cardiomyocyte enlargement is a defining feature of cardiac remodeling. Therefore, the specific role of OTUD7B in cardiac myocytes, treated with either PBS or phenylephrine, was further evaluated by infecting NRCMs with adenoviruses carrying OTUD7B short hairpin RNA (AdshOTUD7B) (Figure 4A). After PBS or phenylephrine treatment for 24 hours, the surface area of the cardiomyocytes was determined by α -actin immunofluorescence staining. Compared with AdshRNA, AdshOTUD7B significantly promoted the enlargement of phenylephrine-induced cardiomyocytes (Figure 4B), and the mRNA expression levels of *NPPA*, *NPPB*, *Myh7*, and *Acta1* were increased (Figure 4C). Furthermore, NRCMs were infected with an adenovirus overexpressing OTUD7B (AdFlag-OTUD7B) (Figure 4D) to elucidate the effects of OTUD7B overexpression on PBS-control or phenylephrine-stimulated CH. However, OTUD7B overexpression significantly reduced cardiomyocyte hypertrophy and downregulated the mRNA expressions of *NPPA*, *NPPB*, *Myh7*, and *Acta1* compared with those in the AdVector phenylephrine control group (Figure 4E and 4F). Nevertheless, α -SMA (α -smooth muscle actin) was not significantly differed from the PBS group in neonatal rat cardiac fibroblasts overexpressing OTUD7B treated with TGF- β (transforming growth factor- β) (Figure S2). These results indicated that OTUD7B attenuated the phenylephrine-induced hypertrophic growth of primary cardiomyocytes.

Role of OTUD7B in the Pathogenesis of CH at the Transcriptomic Level

The role of OTUD7B in the pathogenesis of CH was explored at the transcriptome level by sequencing RNA extracted from the heart tissues of OTUD7B KO and WT mice after TAC. The hierarchical clustering tree revealed that the tissue samples were divided into 2 clusters (Figure 5A). Gene set enrichment analysis showed that fibrosis, heart function, and protein processing-related pathways were all activated by OTUD7B deficiency (Figure 5B). A heat map of the transcriptome analysis demonstrated that OTUD7B deficiency elevated genes encoding fibrosis, myocardial function, and protein expression (Figure 5C). Kyoto Encyclopedia of Genes and Genomes analysis revealed that OTUD7B significantly affected the AKT signaling pathway.

OTUD7B Interacts With KLF4 and Suppresses Its K48-Linked Ubiquitination

Candidate proteins that may bind to OTUD7B were screened to explore the potential mechanisms by which OTUD7B regulates CH. Based on immunoprecipitation-mass spectrometry and RNA sequencing analyses, KLF4 was observed in the front position, which was associated with both the OTUD7B and AKT signaling pathways (Figure 6A). Therefore, the interaction between OTUD7B and KLF4 was investigated further. The transfection of HEK293T cells with Flag-KLF4 and HA-OTUD7B, followed by immunoprecipitation and WB, showed that the exogenous expression of OTUD7B interacted with the exogenous expression of KLF4 (Figure 6B). The endogenous expression of KLF4 and exogenous expression of OTUD7B interacted with each other in NRCMs (Figure 6C). This interaction was further confirmed using the GST pull-down assay (Figure 6D). Series of OTUD7B and KLF4 fragments were constructed to further investigate the binding domains required for interaction between OTUD7B and KLF4. A region of OTUD7B (amino acid [aa] 151-aa446) and a region of KLF4 (aa200-aa397) were required for OTUD7B to bind to KLF4 (Figure 6E). We infected NRCMs with AdFlag-OTUD7B to verify the effect of

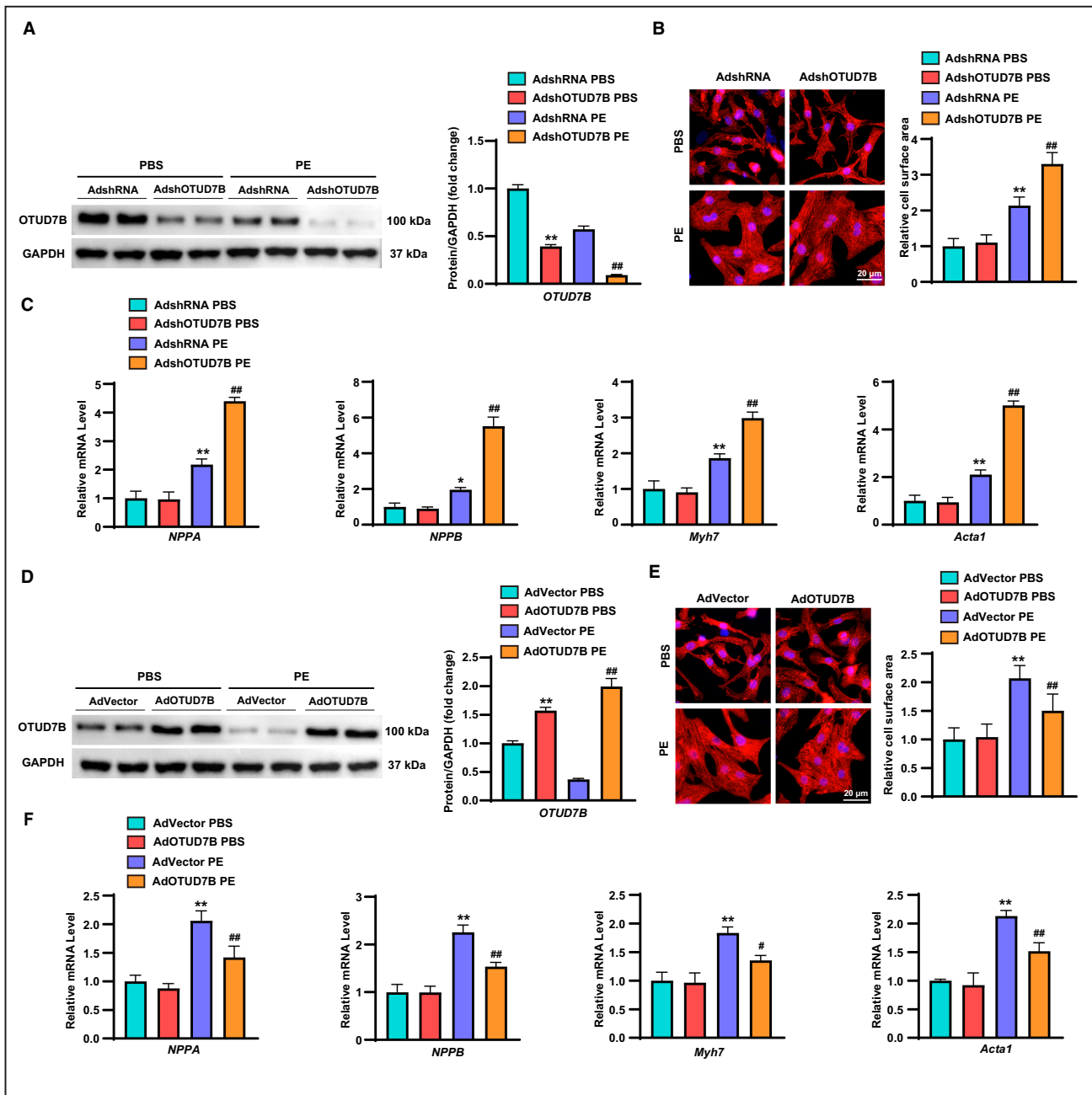


Figure 4. OTUD7B (ovarian tumor domain-containing 7B) deficiency aggravates cardiomyocyte hypertrophy in vitro.

A, Results of AdshRNA or AdshOTUD7B infection with PBS (control)- or phenylephrine (PE)-treated neonatal rat cardiomyocytes (NRCMs) were examined using Western blotting (WB). **B**, Immunofluorescence and quantitative results of the cardiomyocyte size in NRCMs infected with AdshRNA or AdshOTUD7B and treated with PBS or PE for 24 hours. Red: α -actin. Blue: nuclei. Scale bars: 20 μ m. **C**, Reverse transcription-polymerase chain reaction (RT-PCR) analysis of the mRNA levels of *NPPA*, *NPPB*, *Myh7*, and *Acta1* in NRCMs infected with AdshRNA or AdshOTUD7B and treated with PBS or PE for 24 hours. **D**, Results of AdVector or AdOTUD7B infection with PBS-treated or PE-treated NRCMs were examined using WB. **E**, Immunofluorescence and quantitative results of the cardiomyocyte size in NRCMs infected with AdVector or AdOTUD7B and treated with PBS or PE for 24 hours. Red: α -actin. Blue: nuclei. Scale bars: 20 μ m. **F**, RT-PCR analysis of the mRNA levels of *NPPA*, *NPPB*, *Myh7*, and *Acta1* in NRCMs infected with AdVector or AdOTUD7B and treated with PBS or PE for 24 hours. **A** through **F**, * P <0.05 or ** P <0.01 vs AdshRNA PBS or AdVector PBS. # P <0.05 or ## P <0.01 vs AdshRNA PE or AdVector PE. Data are presented as mean \pm SD. Statistical analysis was conducted using 1-way ANOVA. Ad indicates adenovirus; and Adsh, adenovirus vector carrying a short hairpin.

the deubiquitinating enzyme OTUD7B on KLF4 and observed that KLF4 protein expression was substantially upregulated with an increase in AdFlag-OTUD7B

infection (Figure 6F). A KLF4 half-life of 6 to 8 hours was detected in NRCMs using an actinomycin tracking assay, whereas the protein expression level of KLF4

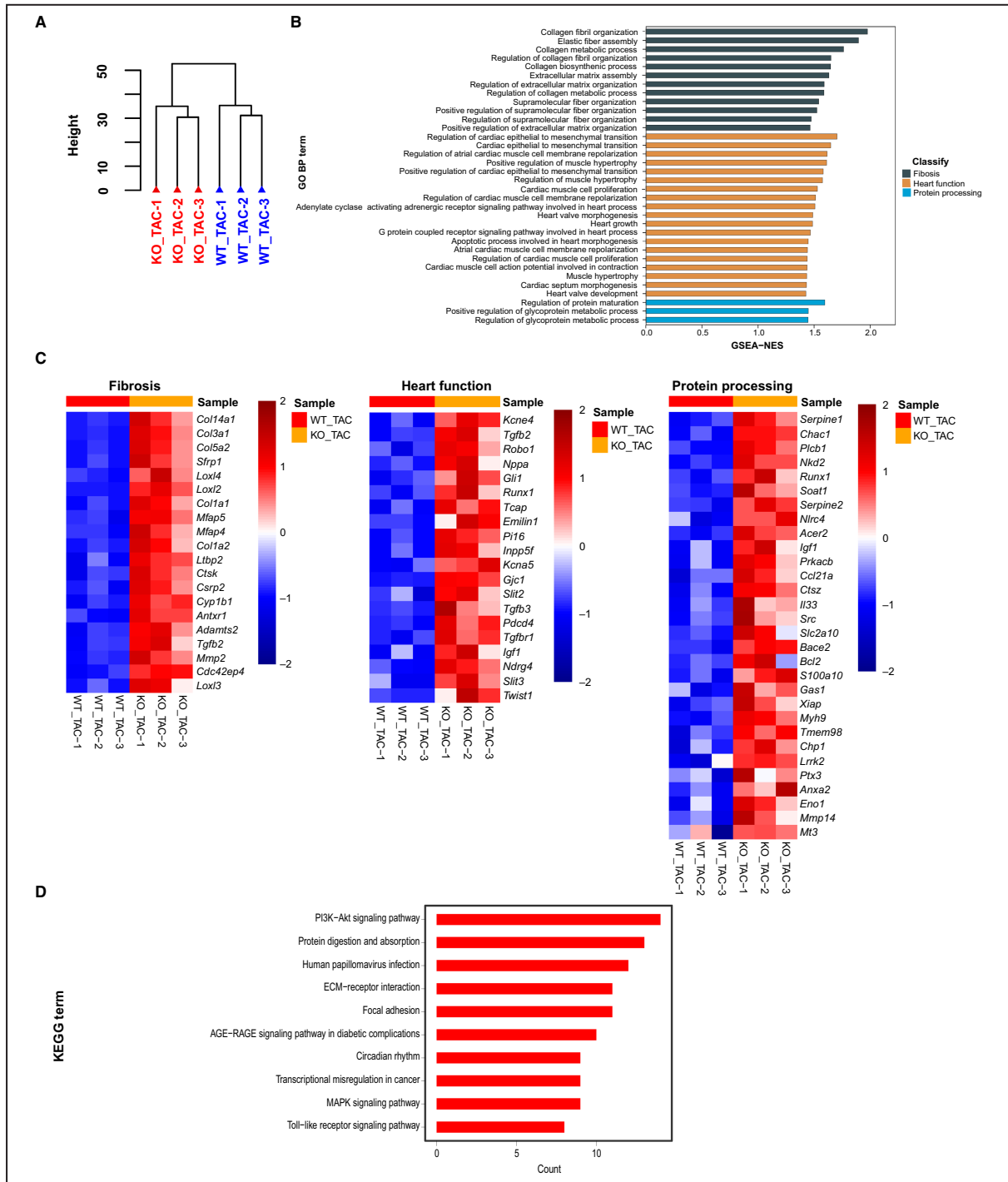


Figure 5. Role of OTUD7B (ovarian tumor domain-containing 7B) in the pathogenesis of cardiac hypertrophy at the transcriptomic level.

A, Hierarchical clustering tree of RNA sequence distribution (n=3 mice per group). **B**, GSEA analysis of RNA-seq data revealed the protein expression pathway activated after OTUD7B deficiency (n=3 mice per group). **C**, Heat map of transcriptome analysis showed that OTUD7B deficiency upregulated genes related to fibrosis, heart function, and protein processing. **D**, KEGG analysis of RNA-seq data showed that OTUD7B deficiency activated the signal pathway of myocardial hypertrophy (n=3 mice per group). AGE-RAGE indicates advanced glycation end products-receptors; ECM, extracellular matrix; GO BP, gene ontology biological process; GSEA, gene set enrichment analysis; KEGG, Kyoto Encyclopedia of Genes and Genomes; KO, knockout; MAPK, mitogen-activated protein kinase; NES, normalized enrichment score; PI3K, phosphatidylinositol 3-kinase; TAC, transverse aortic coarctation; and WT, wild-type.

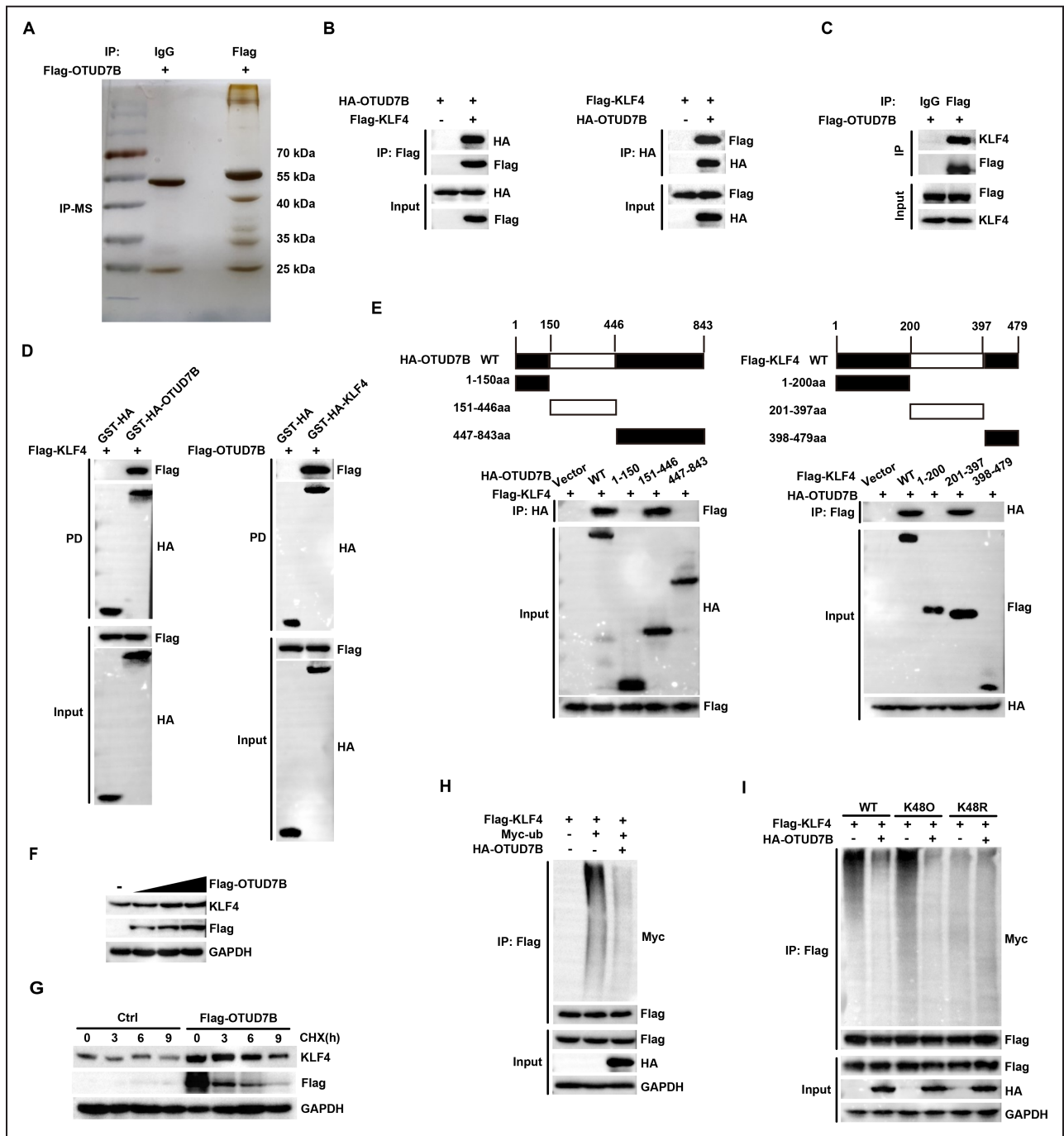


Figure 6. OTUD7B (ovarian tumor domain-containing 7B) interacts with KLF4 and suppresses its K48-linked ubiquitination. **A**, Silver-stained gel showing the indicated molecules and co-immunoprecipitation (IP) using a Flag-OTUD7B and identified using mass spectrometry (MS) in neonatal rat cardiomyocytes (NRCMs). Immunoglobulin G (IgG) was used as the control. **B**, Representative co-IP analyses showed the binding of OTUD7B and KLF4 in human embryonic kidney 293T (HEK293T) cells transfected with Flag-KLF4 and HA-OTUD7B. **C**, Representative endogenous co-IP analyses showed the binding of OTUD7B to KLF4 in NRCMs under phenylephrine (PE) treatment for 12 hours; IgG was used as the control. **D**, Representative GST pull-down assays show direct binding between KLF4 and OTUD7B. Purified GST was used as the control. **E**, Representative Western blotting (WB) for the mapping analyses showed the domains involved in the binding of OTUD7B to KLF4. HEK293T cells were cotransfected with Flag-KLF4 and either full-length HA-OTUD7B or its fragments (left), and representative WB for mapping analyses showed the binding domains of KLF4 to OTUD7B. HEK293T cells were cotransfected with HA-OTUD7B and either full-length Flag-KLF4 or its fragments (right). **F**, WB analysis of KLF4 in NRCMs infected with different amounts of Flag-OTUD7B. **G**, WB analysis of KLF4 in NRCMs infected with Flag-OTUD7B at the indicated time. **H**, Representative IP analysis of KLF4 ubiquitination in HEK 293T cells transfected with the indicated plasmids treated with PE for 12 hours. GAPDH served as a loading control. **I**, Representative IP analysis of KLF4 K48-linked ubiquitination in HEK293T cells transfected with the indicated plasmids treated with PE for 12 hours. GAPDH served as a loading control. CHX(h) indicates cycloheximide; GST, glutathione S-transferase; HA, influenza hemagglutinin epitope; K48, lysine residue at 48 site; and KLF4, Krüppel-like factor 4.

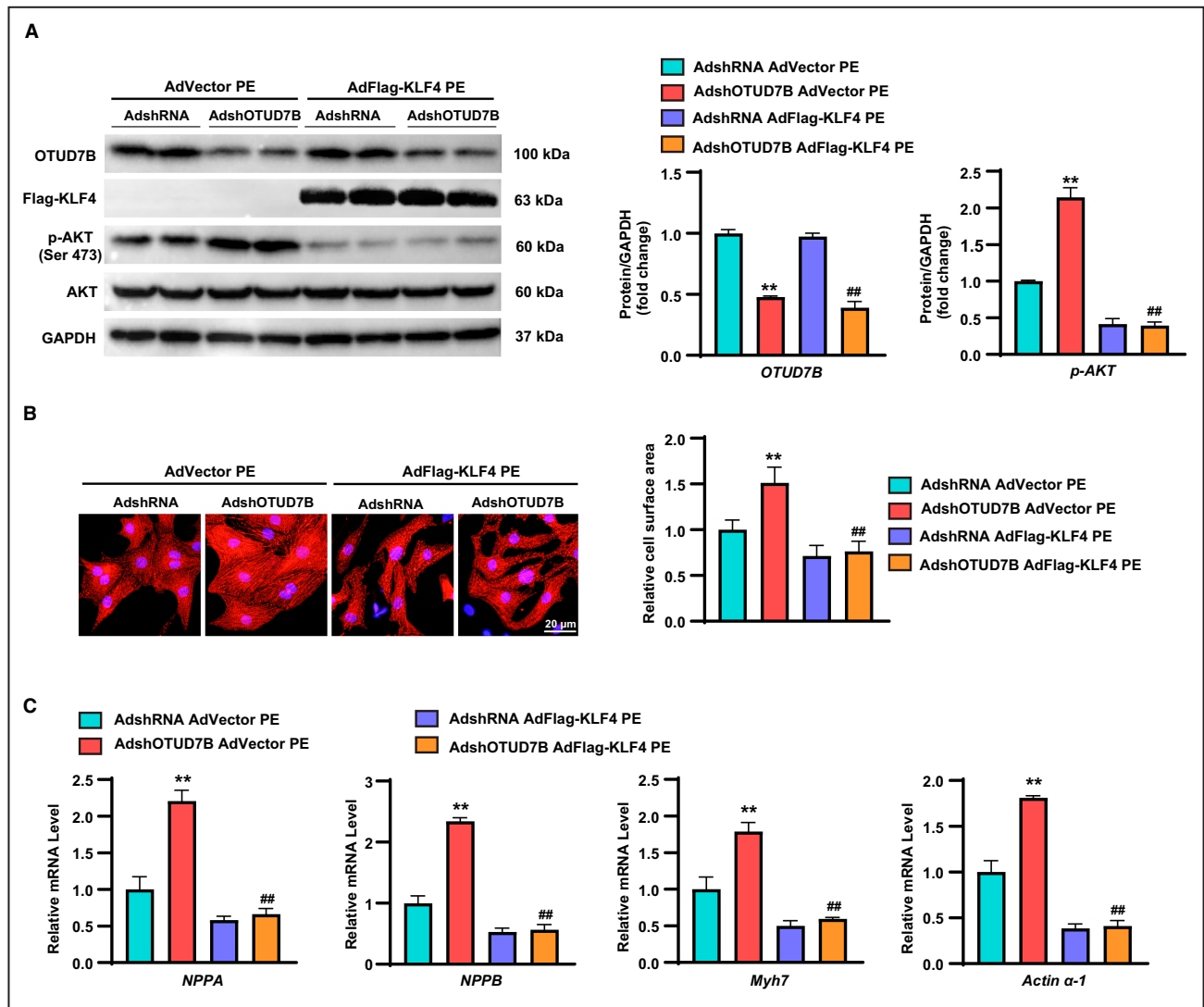


Figure 7. KLF4 (Krüppel-like factor 4) rescues the effects of OTUD7B (ovarian tumor domain-containing 7B) knockdown on cardiac hypertrophy by inhibiting AKT (serine/threonine kinase) phosphorylation.

A, Western blotting analysis of OTUD7B, Flag-KLF4, p-AKT (Ser 473), and AKT in neonatal rat cardiomyocytes (NRCMs) infected with OTUD7B knockdown (AdshOTUD7B) and KLF4 overexpression (AdFlag-KLF4) adenovirus separately or simultaneously and then treated with phenylephrine (PE) for 24 hours. **B**, Immunofluorescence and quantitative results of the cardiomyocyte size in NRCMs infected with OTUD7B knockdown (AdshOTUD7B) and KLF4 overexpression (AdFlag-KLF4) adenovirus separately or simultaneously and then treated with PE for 24 hours. Red: α -actin. Blue: nuclei. Scale bars: 20 μ m. **C**, Reverse transcription-polymerase chain reaction analysis of the mRNA levels of *NPPA*, *NPPB*, *Myh7*, and *Acta1* in NRCMs infected with AdshRNA, AdshOTUD7B, AdVector PE, or AdFlag-KLF4 after PE treatment for 24 hours. **A** through **C**, ** $P < 0.01$ vs AdshRNA AdVector PE. ## $P < 0.01$ vs AdshOTUD7B AdVector PE. Data are presented as mean \pm SD. Statistical analysis was conducted using 1-way ANOVA. AdFlag indicates adenovirus with Flag tag; Adsh, adenovirus vector carrying a short hairpin; and p-AKT, phosphorylated protein kinase B.

was maintained relatively stable upon OTUD7B overexpression (Figure 6G). Further experiments showed that OTUD7B regulated KLF4 stability by affecting its ubiquitination of KLF4 (Figure 6H). The K48-linked polyubiquitin chains were sufficient to target substrate protein degradation during ubiquitin-mediated hydrolysis. The ubiquitination assay revealed that OTUD7B inhibited the addition of K48-linked polyubiquitin chains to maintain KLF4 stability, and the OTUD7B-mediated deubiquitination of KLF4 was abolished when the K48

ubiquitination site was mutated; the mutation information is shown in Table S3 (Figure 6I).

KLF4 Rescues the Effects of OTUD7B Knockdown on CH by Inhibiting AKT Phosphorylation

KLF4 modulates serine/threonine kinase AKT1 signaling in cystic fibrosis.²⁵ We knocked down OTUD7B and overexpressed KLF4, individually or simultaneously, in

phenylephrine-treated NRCMs to investigate whether the function of OTUD7B depends on KLF4 regulating CH through the AKT pathway. WB, immunofluorescence staining, and reverse transcription-polymerase chain reaction demonstrated that the overexpression of KLF4 eliminated the role of the OTUD7B-involved AKT pathway in regulating CH (Figure 7A through 7C). Moreover, KLF4 overexpression inhibits essential differentially expressed genes from RNA sequencing (Figure S3). Collectively, these data suggested that KLF4 acts as a target of OTUD7B and attenuates myocardial hypertrophy via the AKT pathway.

DISCUSSION

The results of this study revealed the regulatory role of OTUD7B in CH. By constructing cellular and animal models of CH, OTUD7B expression was observed to be downregulated. Loss-of-function assays demonstrated that OTUD7B deficiency aggravated TAC-induced CH, mainly by reactivating fetal gene expression, myocardial fibrosis, cardiac remodeling, and dysfunction. Similarly, we observed that OTUD7B overexpression attenuated TAC-induced CH in gain-of-function studies. Our observations indicated that OTUD7B deficiency significantly activated the PI3K-AKT pathway by sequencing RNA extracted from the cardiac tissues of OTUD7B KO mice after TAC surgery. Interestingly, by investigating the molecular mechanism of OTUD7B in CH, OTUD7B was observed to be associated with KLF4 interaction and deubiquitination, which blocked AKT signaling and subsequent CH. Therefore, our study suggested that therapeutic strategies designed for OTUD7B are relevant to pathological CH.

KLF4, which is a member of the KLF (Krüppel-like factor) family, belongs to the C₂H₂-type zinc lipoprotein transcription factor.²⁶ It is localized on chromosome 4B3 and includes aa483 residues in mice.²⁷ The KLF4 protein participates in the regulation of crucial life processes, such as cell proliferation, differentiation, and embryonic development, and it plays a vital role in cell differentiation and cell cycle arrest.²⁸ KLF4-mediated gene transcription involves various posttranslational modifications through phosphorylation, acetylation, methylation, and ubiquitination. These modifications regulate the function of KLF4 by altering its structural stability, DNA-binding capacity, and transcriptional activity.²⁹ KLF4 is a target of HDAC2 (histone deacetylase 2) and inhibits *NPPA* expression in cardiomyocytes, thereby suppressing CH.³⁰ Liao et al have confirmed its role as a key negative regulator of myocardial hypertrophy in vivo.³¹ Additionally, KLF4 inhibits CH occurrence by downregulating cardiac calmodulin expression and activity.³² A previous study showed that the deubiquitinating enzyme USP10 (ubiquitin specific

protease) plays a vital role in lung cancer inhibition via the USP10-KLF4-TIMP3 (tissue inhibitor of metalloproteinase) signaling axis.³³ Saliva-derived miRNAs inhibit vascular remodeling by regulating the OTUD7B/KLF4/NMHC-IIA (non-muscle myosin heavy chain IIA) axis.³⁴ These findings demonstrate that KLF4 mediates the effects of OTUD7B on CH regulation in response to phenylephrine stimulation, which is consistent with our study. Because cardiomyocyte hypertrophy is a defining feature of cardiac remodeling, which is mainly characterized by protein content changes,³⁵ we further investigated the exact role of KLF4 in phenylephrine-induced cardiomyocyte hypertrophy. Phenylephrine-induced CH potentiated by OTUD7B knockdown was completely blocked by the upregulation of KLF4 activity. Moreover, KLF4 upregulation suppressed the upregulated mRNA expression of CH markers in OTUD7B knockdown cells. These findings suggest that KLF4 mediates the regulatory effects of OTUD7B on phenylephrine-stimulated CH. Notably, our study showed that the OTU domain (aa151–aa446) of OTUD7B³⁶ interacted with the transcription repression domain (aa200–aa397) of KLF4, whereas the OTU domain played a major role in deubiquitinating enzyme activity.¹⁶ Moreover, ubiquitination assays revealed that K48-linked polyubiquitin maintained KLF4 stability, which mainly mediated the degradation of target proteins through the ubiquitin/proteasome system and regulated the stability of intracellular proteins.

PI3K/AKT signaling pathway is a key pathway in the process of CH. Overactivation of the PI3K/AKT cascade contributes to the progression of CH in mice overexpressing cardiac-selective transgenic AKT overexpression^{11,37} and in other models of CH.^{38,39} The PI3K-AKT signaling pathway regulates multiple physiological functions, including growth, proliferation, metabolism, angiogenesis, and inflammation, by activating downstream effectors through various compensatory signaling pathways (mainly RAF/MEK/ERK [rapidly accelerated fibrosarcoma/mitogen-activated extracellular signal-regulated kinase/extracellular signal-regulated protein kinase]).⁴⁰ Chronic activation of PI3K, which is a lipid kinase, exacerbates CH and dysfunction, whereas a lack of PI3K diminishes the hypertrophic response to physiological stimuli.⁴¹ CH induced by PI3K activation is associated with downstream AKT, which is a serine/threonine kinase.⁴² Activated AKT in the heart regulates cardiomyocyte size and survival, angiogenic processes, and inflammatory responses through the phosphorylation of downstream targets, including GLUT (facilitative glucose transporter), GSK-3 (glycogen synthase kinase), and mTOR,⁴³ and it plays a pivotal role in the pathogenesis of CH, heart failure, and myocardial infarction.⁴⁴ AKT activity in cardiac tissue contributes to physiological and pathological CH.⁴⁵ PI3K/AKT was shown to be a downstream signaling

pathway of KLF4 in a myocardial hypertrophy study.⁴⁶ Therefore, we assessed AKT expression after KLF4 overexpression and OTUD7B knockdown and observed that phosphorylated AKT was downregulated (Ser 473) in cultured cardiomyocytes.

Our study has some limitations. Due to our insufficient mastery of transgenic mouse construction technology, we did not examine the effect of OTUD7B overexpression on CH in vivo. The inadequacy is currently being considered for further experiments.

CONCLUSIONS

Our study demonstrated that OTUD7B is a negative regulator of pathological CH. Furthermore, it revealed that OTUD7B is a crucial deubiquitinating enzyme that targets and inhibits K48-linked ubiquitination-mediated degradation of KLF4, thus providing a potential therapeutic strategy for CH.

ARTICLE INFORMATION

Received February 13, 2023; accepted August 15, 2023.

Affiliations

Cardiovascular Hospital, The First Affiliated Hospital of Zhengzhou University, Zhengzhou University, Zhengzhou, China (B.-B.D., L.-Y.K., H.-T.S., D.-H.Z., X.W., C.-L.Y., P.-C.L., R.Y., C.L., L.-M.W., Z.H.); and Department of Endocrinology, The First Affiliated Hospital of Zhengzhou University, Zhengzhou University, Zhengzhou, China (J.-L.Z.).

Acknowledgments

B.-B.D., J.-L.Z., L.-Y.K., L.-M.W., and Z.H. participated in research design. All authors conducted experiments, and all authors performed data analysis and interpretation. B.-B.D., J.-L.Z., and L.-Y.K. drafted the article. L.-M.W., and Z.H. supervised the study, and all authors read and approved the final article.

Sources of Funding

This work was supported by grants from the National Natural Science Foundation of China (82200266, 81900333, 82000826), and Excellent Young Natural Science Foundation of Henan Province (232300421055).

Disclosures

None.

Supplemental Material

Tables S1–S3

Figures S1–S3

REFERENCES

- Nakamura M, Sadoshima J. Mechanisms of physiological and pathological cardiac hypertrophy. *Nat Rev Cardiol*. 2018;15:387–407. doi: 10.1038/s41569-018-0007-y
- Zhu L, Li C, Liu Q, Xu W, Zhou X. Molecular biomarkers in cardiac hypertrophy. *J Cell Mol Med*. 2019;23:1671–1677. doi: 10.1111/jcmm.14129
- Tham YK, Bernardo BC, Ooi JY, Weeks KL, McMullen JR. Pathophysiology of cardiac hypertrophy and heart failure: signaling pathways and novel therapeutic targets. *Arch Toxicol*. 2015;89:1401–1438. doi: 10.1007/s00204-015-1477-x
- Zhang Y, Chen W, Wang Y. STING is an essential regulator of heart inflammation and fibrosis in mice with pathological cardiac hypertrophy via endoplasmic reticulum (ER) stress. *Biomed Pharmacother*. 2020;125:110022. doi: 10.1016/j.biopha.2020.110022
- Kumar S, Wang G, Liu W, Ding W, Dong M, Zheng N, Ye H, Liu J. Hypoxia-induced mitogenic factor promotes cardiac hypertrophy via calcium-dependent and hypoxia-inducible factor-1 α mechanisms. *Hypertension*. 2018;72:331–342. doi: 10.1161/HYPERTENSIONAHA.118.10845
- Zhao Q, Song W, Huang J, Wang D, Xu C. Metformin decreased myocardial fibrosis and apoptosis in hyperhomocysteinemia-induced cardiac hypertrophy. *Curr Res Transl Med*. 2021;69:103270. doi: 10.1016/j.retram.2020.103270
- Oldfield CJ, Duhamel TA, Dhalla NS. Mechanisms for the transition from physiological to pathological cardiac hypertrophy. *Can J Physiol Pharmacol*. 2020;98:74–84. doi: 10.1139/cjpp-2019-0566
- Zhao GJ, Zhao CL, Ouyang S, Deng KQ, Zhu L, Montezano AC, Zhang C, Hu F, Zhu XY, Tian S, et al. Ca(2+)-dependent NOX5 (NADPH oxidase 5) exaggerates cardiac hypertrophy through reactive oxygen species production. *Hypertension*. 2020;76:827–838. doi: 10.1161/HYPERTENSIONAHA.120.15558
- Li PL, Liu H, Chen GP, Li L, Shi HJ, Nie HY, Liu Z, Hu YF, Yang J, Zhang P, et al. STEAP3 (six-transmembrane epithelial antigen of prostate 3) inhibits pathological cardiac hypertrophy. *Hypertension*. 2020;76:1219–1230. doi: 10.1161/HYPERTENSIONAHA.120.14752
- Zhang Y, Shang Z, Liu A. Angiotensin-(3-7) alleviates isoprenaline-induced cardiac remodeling via attenuating cAMP-PKA and PI3K/Akt signaling pathways. *Amino Acids*. 2021;53:1533–1543. doi: 10.1007/s00726-021-03074-9
- Ba L, Gao J, Chen Y, Qi H, Dong C, Pan H, Zhang Q, Shi P, Song C, Guan X, et al. Allicin attenuates pathological cardiac hypertrophy by inhibiting autophagy via activation of PI3K/Akt/mTOR and MAPK/ERK/mTOR signaling pathways. *Phytomedicine*. 2019;58:152765. doi: 10.1016/j.phymed.2018.11.025
- Tao H, Xu W, Qu W, Gao H, Zhang J, Cheng X, Liu N, Chen J, Xu GL, Li X, et al. Loss of ten-eleven translocation 2 induces cardiac hypertrophy and fibrosis through modulating ERK signaling pathway. *Hum Mol Genet*. 2021;30:865–879. doi: 10.1093/hmg/ddab046
- Fu D, Zhou J, Xu S, Tu J, Cai Y, Liu J, Cai Z, Wang D, Smilax glabra Roxb. flavonoids protect against pathological cardiac hypertrophy by inhibiting the Raf/MEK/ERK pathway: In vivo and in vitro studies. *J Ethnopharmacol*. 2022;292:115213. doi: 10.1016/j.jep.2022.115213
- Zhao LG, Li PL, Dai Y, Deng JL, Shan MY, Chen B, Zhang KB, Guo SD, Xu ZH. Mibefradil alleviates high-glucose-induced cardiac hypertrophy by inhibiting PI3K/Akt/mTOR-mediated autophagy. *J Cardiovasc Pharmacol*. 2020;76:246–254. doi: 10.1097/FJC.0000000000000844
- Gao L, Yao R, Liu Y, Wang Z, Huang Z, Du B, Zhang D, Wu L, Xiao L, Zhang Y. Isorhamnetin protects against cardiac hypertrophy through blocking PI3K-AKT pathway. *Mol Cell Biochem*. 2017;429:167–177. doi: 10.1007/s11010-017-2944-x
- Hu H, Brittain GC, Chang JH, Puebla-Osorio N, Jin J, Zal A, Xiao Y, Cheng X, Chang M, Fu YX, et al. OTUD7B controls non-canonical NF- κ B activation through deubiquitination of TRAF3. *Nature*. 2013;494:371–374. doi: 10.1038/nature11831
- Xie W, Tian S, Yang J, Cai S, Jin S, Zhou T, Wu Y, Chen Z, Ji Y, Cui J. OTUD7B deubiquitinates SQSTM1/p62 and promotes IRF3 degradation to regulate antiviral immunity. *Autophagy*. 2022;18:2288–2302. doi: 10.1080/15548627.2022.2026098
- Zhang B, Yang C, Wang R, Wu J, Zhang Y, Liu D, Sun X, Li X, Ren H, Qin S. OTUD7B suppresses Smac mimetic-induced lung cancer cell invasion and migration via deubiquitinating TRAF3. *J Exp Clin Cancer Res*. 2020;39:244. doi: 10.1186/s13046-020-01751-3
- Wang B, Jie Z, Joo D, Ordureau A, Liu P, Gan W, Guo J, Zhang J, North BJ, Dai X, et al. TRAF2 and OTUD7B govern a ubiquitin-dependent switch that regulates mTORC2 signalling. *Nature*. 2017;545:365–369. doi: 10.1038/nature22344
- Tang J, Wu Z, Tian Z, Chen W, Wu G. OTUD7B stabilizes estrogen receptor α and promotes breast cancer cell proliferation. *Cell Death Dis*. 2021;12:534. doi: 10.1038/s41419-021-03785-7
- Luo Q, Zhu J, Zhang Q, Xie J, Yi C, Li T. MicroRNA-486-5p promotes acute lung injury via inducing inflammation and apoptosis by targeting OTUD7B. *Inflammation*. 2020;43:975–984. doi: 10.1007/s10753-020-01183-3
- Lin DD, Shen Y, Qiao S, Liu WW, Zheng L, Wang YN, Cui N, Wang YF, Zhao S, Shi JH. Upregulation of OTUD7B (Cezanne) promotes tumor progression via AKT/VEGF pathway in lung squamous carcinoma and adenocarcinoma. *Front Oncol*. 2019;9:862. doi: 10.3389/fonc.2019.00862

23. Mevissen TE, Hospenthal MK, Geurink PP, Elliott PR, Akutsu M, Arnaudo N, Ekkebus R, Kulathu Y, Wauer T, El Oualid F, et al. OTU deubiquitinases reveal mechanisms of linkage specificity and enable ubiquitin chain restriction analysis. *Cell*. 2013;154:169–184. doi: 10.1016/j.cell.2013.05.046
24. Tian S, Jin S, Wu Y, Liu T, Luo M, Ou J, Xie W, Cui J. High-throughput screening of functional deubiquitinating enzymes in autophagy. *Autophagy*. 2021;17:1367–1378. doi: 10.1080/15548627.2020.1761652
25. Sousa L, Pankonien I, Clarke LA, Silva I, Kunzelmann K, Amaral MD. KLF4 acts as a wt-CFTR suppressor through an AKT-mediated pathway. *Cells*. 2020;9:1607. doi: 10.3390/cells9071607
26. Brauer PR, Kim JH, Ochoa HJ, Stratton ER, Black KM, Rosencrans W, Stacey E, Hagos EG. Krüppel-like factor 4 mediates cellular migration and invasion by altering RhoA activity. *Cell Commun Adhes*. 2018;24:1–10. doi: 10.1080/15419061.2018.1444034
27. Wen Y, Lu X, Ren J, Privratsky JR, Yang B, Rudemiller NP, Zhang J, Griffiths R, Jain MK, Nedospasov SA, et al. KLF4 in macrophages attenuates TNF α -mediated kidney injury and fibrosis. *J Am Soc Nephrol*. 2019;30:1925–1938. doi: 10.1681/ASN.2019020111
28. Li L, Zi X, Hou D, Tu Q. Krüppel-like factor 4 regulates amyloid- β (A β)-induced neuroinflammation in Alzheimer's disease. *Neurosci Lett*. 2017;643:131–137. doi: 10.1016/j.neulet.2017.02.017
29. Takeuchi Y, Tatsuta S, Kito A, Fujikawa J, Itoh S, Itoh Y, Akiyama S, Yamashiro T, Wakisaka S, Abe M. Kruppel-like factor 4 upregulates matrix metalloproteinase 13 expression in chondrocytes via mRNA stabilization. *Cell Tissue Res*. 2020;382:307–319. doi: 10.1007/s00441-020-03228-3
30. Jia ZM, Ai X, Teng JF, Wang YP, Wang BJ, Zhang X. p21 and CK2 interaction-mediated HDAC2 phosphorylation modulates KLF4 acetylation to regulate bladder cancer cell proliferation. *Tumour Biol*. 2016;37:8293–8304. doi: 10.1007/s13277-015-4618-1
31. Liao X, Haldar SM, Lu Y, Jeyaraj D, Paruchuri K, Nahori M, Cui Y, Kaestner KH, Jain MK. Krüppel-like factor 4 regulates pressure-induced cardiac hypertrophy. *J Mol Cell Cardiol*. 2010;49:334–338. doi: 10.1016/j.yjmcc.2010.04.008
32. Gu J, Qiu M, Lu Y, Ji Y, Qian Z, Sun W. Piperlongumine attenuates angiotensin-II-induced cardiac hypertrophy and fibrosis by inhibiting Akt-FoxO1 signalling. *Phytomedicine*. 2021;82:153461. doi: 10.1016/j.phymed.2021.153461
33. Wang X, Xia S, Li H, Wang X, Li C, Chao Y, Zhang L, Han C. The deubiquitinase USP10 regulates KLF4 stability and suppresses lung tumorigenesis. *Cell Death Differ*. 2020;27:1747–1764. doi: 10.1038/s41418-019-0458-7
34. Yang GS, Zheng B, Qin Y, Zhou J, Yang Z, Zhang XH, Zhao HY, Yang HJ, Wen JK. Salvia miltiorrhiza-derived miRNAs suppress vascular remodeling through regulating OTUD7B/KLF4/NMHC IIA axis. *Theranostics*. 2020;10:7787–7811. doi: 10.7150/thno.46911
35. Wang ZV, Hill JA. Protein quality control and metabolism: bidirectional control in the heart. *Cell Metab*. 2015;21:215–226. doi: 10.1016/j.cmet.2015.01.016
36. Mevissen TET, Kulathu Y, Mulder MPC, Geurink PP, Maslen SL, Gersch M, Elliott PR, Burke JE, van Tol BDM, Akutsu M, et al. Molecular basis of Lys11-polyubiquitin specificity in the deubiquitinase cezanne. *Nature*. 2016;538:402–405. doi: 10.1038/nature19836
37. Yan L, Wei X, Tang QZ, Feng J, Zhang Y, Liu C, Bian ZY, Zhang LF, Chen M, Bai X, et al. Cardiac-specific mindin overexpression attenuates cardiac hypertrophy via blocking AKT/GSK3 β and TGF- β 1-Smad signalling. *Cardiovasc Res*. 2011;92:85–94. doi: 10.1093/cvr/cvr159
38. Meng X, Cui J, He G. Bcl-2 is involved in cardiac hypertrophy through PI3K-Akt pathway. *Biomed Res Int*. 2021;2021:6615502. doi: 10.1155/2021/6615502
39. Magaye RR, Savira F, Hua Y, Xiong X, Huang L, Reid C, Flynn BL, Kaye D, Liew D, Wang BH. Attenuating PI3K/Akt-mTOR pathway reduces dihydrosphingosine 1 phosphate mediated collagen synthesis and hypertrophy in primary cardiac cells. *Int J Biochem Cell Biol*. 2021;134:105952. doi: 10.1016/j.biocel.2021.105952
40. Wang HB, Huang SH, Xu M, Yang J, Yang J, Liu MX, Wan CX, Liao HH, Fan D, Tang QZ. Galangin ameliorates cardiac remodeling via the MEK1/2-ERK1/2 and PI3K-AKT pathways. *J Cell Physiol*. 2019;234:15654–15667. doi: 10.1002/jcp.28216
41. Fan C, Li Y, Yang H, Cui Y, Wang H, Zhou H, Zhang J, Du B, Zhai Q, Wu D, et al. Tamarixetin protects against cardiac hypertrophy via inhibiting NFAT and AKT pathway. *J Mol Histol*. 2019;50:343–354. doi: 10.1007/s10735-019-09831-1
42. Xue JF, Shi ZM, Zou J, Li XL. Inhibition of PI3K/AKT/mTOR signalling pathway promotes autophagy of articular chondrocytes and attenuates inflammatory response in rats with osteoarthritis. *Biomed Pharmacother*. 2017;89:1252–1261. doi: 10.1016/j.biopha.2017.01.130
43. Marquard FE, Jücker M. PI3K/AKT/mTOR signaling as a molecular target in head and neck cancer. *Biochem Pharmacol*. 2020;172:113729. doi: 10.1016/j.bcp.2019.113729
44. Hermida MA, Dinesh Kumar J, Leslie NR. GSK3 and its interactions with the PI3K/AKT/mTOR signalling network. *Adv Biol Regul*. 2017;65:5–15. doi: 10.1016/j.jbior.2017.06.003
45. Schüttler D, Clauss S, Weckbach LT, Brunner S. Molecular mechanisms of cardiac remodeling and regeneration in physical exercise. *Cells*. 2019;8:1128. doi: 10.3390/cells8101128
46. Yang Y, Wang Z, Yao M, Xiong W, Wang J, Fang Y, Yang W, Jiang H, Song N, Liu L, et al. Oxytocin protects against isoproterenol-induced cardiac hypertrophy by inhibiting PI3K/AKT pathway via a lncRNA GAS5/miR-375-3p/KLF4-dependent mechanism. *Front Pharmacol*. 2021;12:766024. doi: 10.3389/fphar.2021.766024